Broken-Symmetry and Approximate Spin-Projected Potential Energy Curves for Bimetallic Systems: A Density Functional Study of M_2Cl_9, M = Cr^{III}, Mo^{III}, W^{III}, and Re^{IV}

John E. McGrady, Robert Stranger,* and Timothy Lovell

Department of Chemistry, The Faculties, The Australian National University, Canberra, ACT 0200, Australia

Received: August 20, 1996; In Final Form: June 13, 1997[⊗]

Potential energy curves for the title compounds are examined using broken-symmetry approximate density functional theory. Three distinct regions can be identified, depending on which subsets (σ or δ_π) of the metal-based valence electrons are delocalized, and the position of the global minimum is determined by the relative stabilities of these three regions. Approximate spin-projection techniques are employed to obtain pure singlet ground-state energies. When only the weakly coupled electrons are included in the projection, the pure singlet ground-state curve closely follows that of the broken-symmetry state at all points. In contrast, if strongly coupled electrons are included in the projection, the stability of the pure singlet state is overestimated, leading to artifacts in the potential energy curve. Using the local density approximation (LDA), *r*M−M is estimated to within 0.1 Å of the experimental range for the $Cr_2Cl_9^{3-}$, $W_2Cl_9^{3-}$, and $Re_2Cl_9^{1-}$ systems. In contrast, the optimized Mo−Mo separation for $Mo_2Cl_9^{3-}$ is smaller than any of the crystallographically determined values. This may reflect the flatness of the potential energy curve in the vicinity of the minimum, which allows the structure of the anion to change in response to the presence of cations in the crystal. Gradient corrections underestimate the strength of metal−metal bonding, leading to unreasonably long metal−metal separations in all cases, while quasi-relativistic effects in the tungsten and rhenium systems have the opposite effect, increasing the strength of the metal−metal bonding.

Introduction

The nature of metal−metal interactions in bimetallic systems remains a topic of enduring interest.[1] The metal nonahalides $M_2X_9^{z-}$ represent a particulary important class of complexes, because examples are known for a wide variety of transition metal ions, and the series provides a unique opportunity to study periodic trends in metal−metal bonding within a constant ligand environment.[2] The structures of the nonachlorides of the chromium triad exemplify periodic trends in metal−metal bonding, with the metal−metal separation increasing from approximately 2.45 Å for $W_2Cl_9^{3-}$ to 3.10 Å for the chromium congener, indicating significantly stronger metal−metal bonding in the former. Despite the structural differences, both of these complexes are diamagnetic at low temperatures, indicating that a spin singlet ground state may arise from very different extremes of metal−metal bonding. At one limit, the electrons may be fully delocalized over both metal ions, thereby forming a triple bond. Alternatively, they may remain localized on one center or the other, in which case the spin singlet arises through relatively weak antiferromagnetic coupling. Between these two extremes lies a continuum of intermediate situations, where the metal-based electrons are neither fully localized or delocalized. If we wish to study periodic trends in metal−metal bonding, we clearly need a computational technique which can encompass both localized and delocalized situations, as well as the intermediate cases, without making any *a priori* assumptions regarding the nature of the metal−metal bond.

If the two metal centers in a dimer are related by a symmetry element of the relevant point group, then each electron must necessarily have equal amplitude at both centers, and a delocalized solution is imposed on the system. Thus we see immediately that such "full-symmetry" calculations are unable to encompass the weakly coupled limit, where the electrons are fully localized. In contrast, if all symmetry elements connecting the two metal centers are removed, and the calculation performed in a spin-unrestricted manner, individual electrons may localize on one center or the other, but will only do so if such a situation is energetically favored over the delocalized alternative. The so-called "broken-symmetry" approach, developed by Noodleman and co-workers,[3] therefore encompasses both weak antiferromagnetic coupling and strong metal−metal bonding modes, as well as the continuum of intermediate situations—precisely the criteria defined above as necessary for exploring periodic trends in bonding. Calculations using this technique have now been applied with great success to a wide variety of main-group[4] and transition-metal-based systems.[5,6]

In a recent communication, we reported optimized metal−metal separations for $M_2Cl_9^{3-}$, M = Cr, Mo, and W, using approximate density functional theory (DFT).[7] In $Cr_2Cl_9^{3-}$, the metal−metal interaction is very weak, and the spin-up and spin-down electrons occupying the Cr 3d orbitals remain completely localized on one center or the other. Accordingly, the equilibrium Cr−Cr separation could be adequately modelled only by "breaking" the molecular symmetry from D_{3h} to C_{3v}. Calculations performed in full D_{3h} symmetry underestimated the Cr−Cr separation by almost 1.0 Å. In contrast, the metal-based orbitals in $W_2Cl_9^{3-}$ are completely delocalized due to strong metal−metal bonding, and the experimentally observed W−W separation was reproduced to within 0.05 Å by calculations in both D_{3h} and C_{3v} symmetry. In this paper we extend these preliminary results by considering in detail the nature of the broken-symmetry potential energy curves (in the range 2.0 < *r*M−M < 3.8 Å) of four isoelectronic systems, $Cr_2Cl_9^{3-}$, $Mo_2Cl_9^{3-}$, $W_2Cl_9^{3-}$, and $Re_2Cl_9^{1-}$. In addition to the local density approximation (LDA) considered previously, we evaluate the importance of gradient corrections to the LDA and also that of quasi-relativistic corrections in complexes of the third transition series elements (W and Re).

[⊗] Abstract published in *Advance ACS Abstracts,* August 1, 1997.

S1089-5639(96)02556-X CCC: $14.00

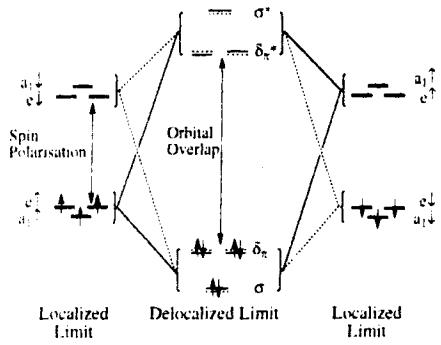

Figure 1. Representation of the broken-symmetry state of $M_2Cl_6^{n-}$ in both localized and delocalized limits. Orbitals are labeled according to the representations of the C_{3v} point group.

The gross features of the metal−metal interaction in a confacial bioctahedron can be derived from a consideration of the electronic structure of the component metal ions.[8] The t_{2g}-based orbitals of each metal ion split into a_1 and e subsets (labeled according to the representations of the C_{3v} point group), the former having σ symmetry with respect to the trigonal axis, while the latter have mixed δ and π (denoted δ_π) symmetry (Figure 1). In the limit of very weak metal−metal bonding, each of these single-ion orbitals remains localized on one center (Figure 1, localized limit). The spin polarization energy associated with the presence of an excess of spin-up or spin-down electron density causes a splitting of the t_{2g} manifold. As the overlap of the metal-based orbitals on each center increases, bonding and antibonding molecular orbitals are formed. In the limit of full delocalization (Figure 1, delocalized limit), the spin-polarization splitting is lost, but the orbitals are now split by significant bonding (σ and δ_π) and antibonding (σ^* and δ_π^*) character. The point at which the transition from localized to delocalized behavior occurs will clearly depend on the orientation of the orbital in question. The overlap of the σ orbitals is clearly much greater than that of their counterparts of δ_π symmetry. All other factors being equal, we would therefore anticipate that the σ electrons would tend to delocalize more readily than δ_π.

Computational Details

All approximate density functional[9] calculations reported in this work were performed using the Amsterdam density functional (ADF) program version 2.0.1.[10] A double-ζ Slater type orbital basis set extended with a single d-polarization function was used to describe chlorine, while all metals were modelled with triple-ζ basis sets. Electrons in orbitals up to and including 2p {Cl}, 3p {Cr}, 4p {Mo}, and 5p {W, Re} were considered to be part of the core and treated in accordance with the frozen-core approximation. Calculations were performed using three distinct exchange−correlation functionals, denoted LDA, BP, and PW91. The LDA approximation includes the local exchange−correlation potential of Vosko, Wilk, and Nusair.[11] BP incorporates the gradient corrections to the exchange (Becke)[12] and correlation (Perdew)[13] functionals, while the PW91 functional incorporates the more recent gradient corrections to exchange and correlation of Perdew et al.[14] The influence of the quasi-relativistic corrections[15] was also considered for tungsten and rhenium complexes. The individual points on the potential energy curves for the broken-symmetry ground state were calculated by freezing the metal−metal separation, rM−M, at 0.1 Å intervals between 1.8 and 3.8 Å. All other independent structural parameters were optimized using the gradient algorithm of Versluis and Ziegler.[16] Single-point calculations were then performed at the optimized geometries to obtain the energies of the corresponding $S = 0$, 2, and 3 states.

Results and Discussion

Qualitative Features of the Potential Energy Curves. The broken-symmetry state arising from interaction of the two metal centers may be defined, without making any assumptions regarding the extent of delocalization of the electrons, by the configuration $(a_1\uparrow)^1(a_1\downarrow)^1(e\uparrow)^2(e\downarrow)^2(e\uparrow)^0(e\downarrow)^0(a_1\uparrow)^0(a_1\downarrow)^0$ (Figure 1). In the weakly coupled limit, both σ and δ_π orbitals remain localized on one center or the other, while in the strongly coupled limit, both subsets are fully delocalized and correlate with the corresponding orbitals of the D_{3h} point group. Given the previous discussion of the angular properties of the σ and δ_π orbitals, we anticipate that at some intermediate point the σ electrons will delocalize while their δ_π counterparts will remain localized, giving rise to an effective metal−metal single bond. We can therefore identify three distinct bonding modes, depending on which subsets of the metal-based electrons are localized/delocalized, all of which are consistent with the single determinant broken-symmetry wave function described above. Therefore, the broken-symmetry potential energy curve should make a smooth transition from one region to the next as the metal−metal separation is varied.

The simplest way to determine which bonding regime is prevalent at any point in the broken-symmetry curve is to define a series of "associated" states. If a subset of metal-based electrons is weakly coupled in the broken-symmetry state, then an obvious corollary is that the state in which the same electrons are decoupled (*i.e.*, coupled ferromagnetically) must lie close in energy. For example, if all metal based electrons (σ and δ_π) are localized in the broken-symmetry state (corresponding to weak antiferromagnetic coupling of two single ions of spin $S = {}^3/_2$), then the associated $S = 3$ state, corresponding to ferromagnetic coupling of the same electrons, must lie close in energy. This $S = 3$ state is defined by the single determinant wave function $(a_1\uparrow)^1(a_1\downarrow)^0(e\uparrow)^2(e\downarrow)^0(e\uparrow)^2(e\downarrow)^0(a_1\uparrow)^1(a_1\downarrow)^0$. Similarly, if the σ electrons are strongly coupled (delocalized), but the δ_π subset remain weakly coupled, then the ferromagnetic state in which only the δ_π electrons are uncoupled will lie close to the broken-symmetry state. This associated state, $S = 2$, is defined by the configuration $(a_1\uparrow)^1(a_1\downarrow)^1(e\uparrow)^2(e\downarrow)^0(e\uparrow)^2(e\downarrow)^0(a_1\uparrow)^0(a_1\downarrow)^0$. Finally, in the limit of full delocalization, the broken-symmetry state corresponds exactly to the ground-state calculated using the full molecular symmetry of D_{3h}, defined by the configuration $(a_1'\uparrow)^1(a_1'\downarrow)^1(e'\uparrow)^2(e'\downarrow)^2(e''\uparrow)^0(e''\downarrow)^0(a_2''\uparrow)^0(a_2''\downarrow)^0$. The use of symmetry labels appropriate to the D_{3h} point group indicates that in this case delocalization has been enforced by the use of full symmetry. By considering the energies of the associated states, $S = 0$, 2, and 3, it is possible to define the nature of the metal−metal bonding at any point on the broken-symmetry curve.

Approximate Spin Projection of the Pure Singlet Ground State. In the absence of complete delocalization of all metal-based electrons, the broken-symmetry state does not correspond to a pure singlet ground state, but rather to a weighted average of the pure spin states arising from coupling of the two single ions. This spin-contamination problem can be addressed using the approximate spin projection technique developed by Noodleman.[17] This method requires the computation of the energy of the antiferromagnetic broken-symmetry state described above, E_B, and also that of the ferromagnetic state $E(S_{max})$. From these two energies, the Heisenberg exchange coupling constant, J can

be obtained using the expression

$$E(S_{max}) - E_B = -S^2_{max} J \quad (1)$$

The energy of the pure singlet ground state $E(0)$ is given by

$$E(S_{max}) - E(0) = -S_{max}(S_{max} + 1)J \quad (2)$$

and so, from eqs 1 and 2, $E(0)$ can be expressed as

$$E(0) = [(S_{max} + 1)E_B - E(S_{max})]/S_{max} \quad (3)$$

The principal difficulty in applying eq 3 lies in the selection of the appropriate high-spin state S_{max}. It is important to note that eq 1 (and, therefore, eq 3) applies only to weakly antiferromagnetically coupled electrons, and it becomes increasingly less valid as the electrons become involved in strong metal−metal bonds. We therefore need to make a decision as to which electrons we treat as weakly coupled and which we regard as being involved in strong metal−metal bonds. This problem was noted in a recent publication discussing the electronic structure of Cr_2,[5a] where pure singlet ground-state energies $E(0)$ were extracted assuming that all five d electrons per chromium atom could be treated as weakly coupled across the whole potential energy curve. The potential limitations of assuming $S_{max} = 5$ throughout were noted, but no attempt was made to evaluate the validity of the assumption across a range of rCr−Cr.

In the metal nonahalides considered in this paper, S_{max} must correspond to one of the associated states, $S = 0$, 2, or 3, defined in the previous section. In the limit of weak antiferromagnetic coupling, the maximum spin state will clearly correspond to decoupling of all six d electrons, $S = 3$. In the intermediate region, where the σ electrons are effectively factored out in a strong bond, only the δ_π electrons are weakly coupled, and in this case the maximum spin state corresponds to $S = 2$. Finally in the limit of full delocalization, the broken- and full-symmetry ($S = 0$) states converge, and no correction is necessary to obtain the pure singlet ground-state energy. Thus we anticipate that the value of S_{max} in eq 3 will vary across the potential energy curve, and will most readily be determined by consideration of the proximity of the three associated spin states defined above to the broken-symmetry curve.

Potential Energy Curves for $Cr_2Cl_9^{3-}$, $W_2Cl_9^{3-}$, $Re_2Cl_9^{1-}$, and $Mo_2Cl_9^{3-}$. The potential energy curves for the broken-symmetry states of the four complexes, calculated using the LDA, are shown in bold in Figures 2−5. The curves for the associated $S = 0$, 2, and 3 states are also shown, as are the spin-projected ground states, calculated using eq 3 and assuming either $S_{max} = 2$ or 3. The variation in net spin density, defined by the difference in spin-up and spin-down Mulliken electron densities at each metal center, is also shown in each figure. Optimized metal−metal separations and total energies of the broken-symmetry and associated states are summarized in Table 1.

$Cr_2Cl_9^{3-}$. Cr−Cr separations in $A_3Cr_2Cl_9$ complexes range from 3.05 to 3.12 Å, depending on the identity of the cation, and magnetic studies indicate that the two chromium centers are only very weakly antiferromagnetically coupled.[18] The net spin density shown in Figure 2 remains above 3.0 for all rCr−Cr > 2.7 Å, confirming that, in the region of the global minimum (rCr−Cr = 3.22 Å), the electrons remain almost completely localized. Accordingly, the $S = 3$ associated state converges with the broken-symmetry curve above 2.7 Å. At smaller internuclear separations, the coupling of the metal-based electrons increases, the σ^* orbital acquires significant antibonding character, and the $S = 3$ state, in which this orbital is occupied, is destabilized relative to the broken-symmetry state, in which it is not. An important point emerges from this discussion: the region where the broken-symmetry and $S = 3$ curves lie parallel and close to each other represents the region in which all six metal-based electrons are weakly coupled in the broken-symmetry state. The point at which the two curves diverge marks the metal−metal separation where the σ electrons begin to delocalize in the broken-symmetry state and hence where weak antiferromagnetic coupling of both σ and δ_π subsets is no longer a valid description of the bonding in this state. As the $S = 3$ curve begins to move to higher energy, the $S = 2$ state drops and converges toward the broken-symmetry state in the region where 2.1 < rCr−Cr < 2.6 Å. This in turn indicates that the broken-symmetry state is now best formulated as arising from weak antiferromagnetic coupling of the δ_π electrons, but strong coupling of the σ manifold (*i.e.*, an effective Cr−Cr single bond is present). Finally, at even lower Cr−Cr separations (< 2.1 Å), the δ_π electrons delocalize, conferring significant antibonding character on the δ_π^* orbital. Accordingly, the $S = 2$ state, in which δ_π^* is doubly occupied, moves to higher energy than the broken-symmetry curve, where it is vacant. At the same time, the $S = 0$ curve, calculated using D_{3h} symmetry, converges with the broken-symmetry state, confirming that the metal-based electrons are all fully delocalized.

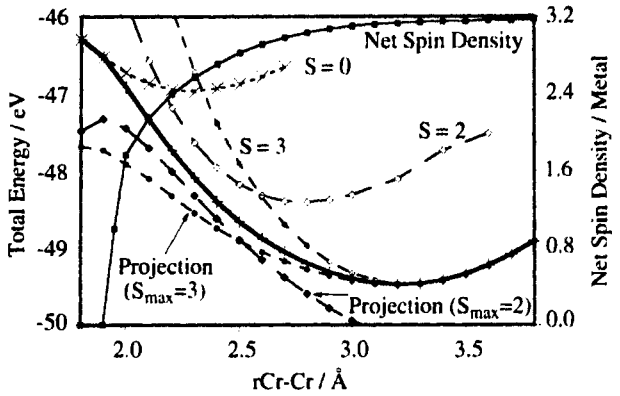

Figure 2. Potential energy curves for broken-symmetry, associated and spin-projected states of $Cr_2Cl_9^{3-}$. The broken-symmetry state is shown in bold.

In the previous section, the divergence to higher energy (relative to the broken-symmetry state) of the $S = 2$ and $S = 3$ states as rCr−Cr is reduced was traced to the development of significant antibonding character in the δ_π^* and σ^*, which are occupied in the higher spin states. At the opposite extreme, the $S = 0$ and $S = 2$ states also diverge to higher energy at large rCr−Cr. In the limit of large metal−metal separation, the single determinant wave functions defining the $S = 3$, 2, and 0 states correlate with single-ion spin states of $^3/_2$, 1, and 0 respectively. The stabilities of these single-ion states decrease in the order $S = {}^3/_2 > S = 1 > S = 0$, in accord with Hund's rule, and hence the $S = 3$ associated state ($2S = {}^3/_2$) is always the most stable at large internuclear separations. A significant point emerges from this discussion: an intermediate spin state such as $S = 2$ will lie close to a broken-symmetry state only over a narrow range of metal−metal separations, and the spin state *must* necessarily diverge to *higher* energy at both smaller and larger distances. This point will have very important implications for the approximate spin projection procedure described below.

To summarize, we can identify three distinct regions in the potential energy curve of $Cr_2Cl_9^{3-}$. At large rCr−Cr, the lowest

energy associated state is $S = 3$, indicating localization of both σ and δ_π electrons. At smaller internuclear separations, the lowest energy state is $S = 2$, indicating delocalized σ electrons, while the δ_π electrons remain localized. Finally, at even lower rCr−Cr, both σ and δ_π electrons are delocalized, and the $S = 0$ state lies lowest. The broken-symmetry state follows the path of lowest energy between the three associated states, thereby making a smooth transition from one region to the next.

Having described the appearance of the broken-symmetry curve, along with that of the associated $S = 0$, 2, and 3 states, we are now in a position to discuss the energy of the pure singlet ground state obtained by approximate spin projection using eq 3. At this point we reiterate that eq 3 is valid only when the two single ions are *weakly* antiferromagnetically coupled. As noted previously, we could make two possible projections, using either $S_{max} = 2$ or $S_{max} = 3$, depending on which subsets of electrons we choose to regard as weakly coupled. From our previous discussion, it now becomes clear that projection using $S_{max} = 3$ will only be valid where the associated $S = 3$ state lies close in energy to that for the broken-symmetry state. Therefore, for rCr−Cr > 2.7 Å, the $S_{max} = 3$ projected ground state provides the most accurate estimate of the pure singlet ground-state energy. In contrast, in the region 2.0 < rCr−Cr < 2.6 Å, the $S = 2$ state lies parallel to the broken-symmetry curve, and spin projection using $S_{max} = 2$ is more appropriate than $S_{max} = 3$. Finally, where rCr−Cr < 2.1 Å, the $S = 0$ curve converges with the broken-symmetry state and all electrons are delocalized. In this case there is no spin contamination in the calculated ground state, and so no spin projection is required.

With these guidelines in mind, we see that the $S_{max} = 3$ spin-projected ground state closely follows the broken-symmetry curve in the region 2.7 < rCr−Cr < 3.8 Å, and then diverges to lower energy. Similarly, where 2.1 < rCr−Cr < 2.6 Å, the $S_{max} = 2$ projected curve closely follows the broken-symmetry curve. This is in fact nothing more than a simple corollary of the statement that eq 3 is only valid for weakly coupled electrons: the energy correction is a multiple of J, the exchange coupling constant, so if J must be small, then the correction to the energy must also be relatively small. The only regions which cannot be treated using the simple perturbative treatment embodied in eq 3 are those where the transition between two well-defined sections of the spin-projected curves occurs, around rCr−Cr = 2.0 Å and rCr−Cr = 2.6 Å. In these situations, the degree of delocalization is changing rapidly as a function of metal−metal separation, S_{max} is nonintegral, and the high-spin state cannot be accurately defined by a single configuration. Nevertheless, simple interpolation between the well-defined regions of the spin-projected curves results in a smooth "hybrid" curve which closely follows the broken-symmetry curve at all points. In marked contrast, if a particular projection scheme is used outside the region in which it is valid, the calculated ground-state must diverge to lower energy. Thus incorrect spin projection will necessarily lead to overestimation of the spin-projected ground-state energy and hence to artifacts such as secondary minima in the potential energy curve.

The detailed discussion of spin projection given above is not intended to present our hybrid projection scheme as one of general utility, to be applied routinely to other systems. In fact, we wish to illustrate just the opposite, that, when applied in a realistic manner, the spin-projected ground state *must* lie close to the broken-symmetry curve at all points and hence the latter always gives a good estimate of the true ground-state energy. Indeed if significant divergence of the broken-symmetry and spin-projected curves does occur, as was observed in previous

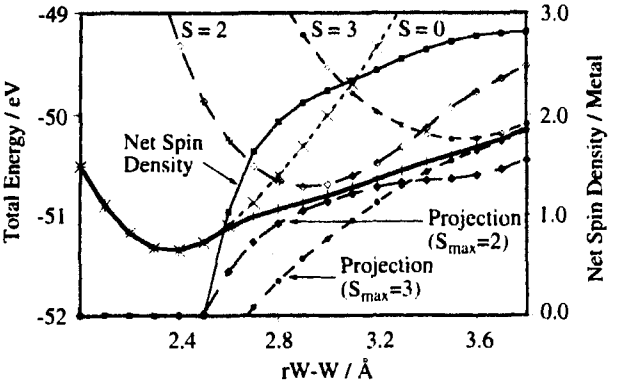

Figure 3. Potential energy curves for various states of $W_2Cl_9^{3-}$.

work on Cr_2,[5a] this should immediately raise suspicions that the assumptions made in applying eq 3 may be invalid.

$W_2Cl_9^{3-}$. In contrast to $Cr_2Cl_9^{3-}$, the metal−metal bond in $W_2Cl_9^{3-}$ is short (2.42−2.50 Å)[19] indicating the presence of strong W−W bonding. The LDA potential energy curves for $W_2Cl_9^{3-}$ are illustrated in Figure 3. As in Figure 2, the broken-symmetry state is shown in bold, and the $S = 0$, 2, and 3 associated states and the corresponding spin-projected ground states are also shown. The general features of the broken-symmetry curve may be interpreted in similar fashion to those of $Cr_2Cl_9^{3-}$, using the associated states as a guide. At large rW−W, the $S = 3$ state lies close and parallel to the broken-symmetry state, indicating that all metal-based electrons are weakly coupled. In the region 2.8 < rW−W < 3.4 Å, the $S = 2$ curve converges on the broken-symmetry state, indicating the presence of a W−W single bond, while below 2.8 Å the broken-symmetry state is identical to $S = 0$, indicating full electron delocalization.

Comparing the minima of the associated states (Table 1), it is clear that their positions along the rM−M axis are relatively independent of the identity of the metal ion, and the major difference between tungsten and chromium arises simply in the relative energies of the $S = 0$, 2, and 3 states. For $Cr_2Cl_9^{3-}$, the energy of the states increases in the order $S = 3 < S = 2 < S = 0$, and hence the global minimum on the broken-symmetry curve corresponds to the antiferromagnetic counterpart of the $S = 3$ state (*i.e.*, weak coupling of all metal-based electrons). In contrast, the ordering of the associated states for $W_2Cl_9^{3-}$ is reversed ($S = 0 < S = 2 < S = 3$), and the global minimum corresponds to the fully delocalized state with short rW−W. The difference between chromium and tungsten is caused by the more diffuse d orbitals of the latter. At any particular internuclear separation, the larger 5d orbitals afford more effective σ and δ_π overlap than the 3d orbitals of chromium, stabilizing the $S = 0$ associated state. At the same time, the smaller orbitals of chromium reduce the average interelectron separation, thereby increasing the spin polarization energy, and stabilising the spin-quartet single-ion states present in $S = 3$. A detailed analysis of the relative contributions of these two distinct terms to periodic trends in bonding is the subject of another paper.[20]

The spin projection procedure must again be considered in three distinct regions, corresponding to the three different coupling modes. For rW−W > 3.4 Å, projection using $S_{max} = 3$ gives the best approximation to the pure singlet ground state, while in the range 2.8 Å < rW−W < 3.4 Å, $S_{max} = 2$ is appropriate. Finally, below rW−W = 2.8 Å, the broken-symmetry state converges to the fully delocalized limit, and no spin projection is required. In each region, the broken-symmetry state again lies very close to the spin-projected ground state,

TABLE 1: Optimized Metal–Metal Separations (Å) of the Broken-Symmetry and Associated States of $Cr_2Cl_9^{3-}$, $Mo_2Cl_9^{3-}$, $W_2Cl_9^{3-}$, and $Re_2Cl_9^{1-}$

	LDA	PW	BP	QR/LDA	QR/PW	QR/BP	exptl
$Cr_2Cl_9^{3-}$							
broken symmetry	3.22 (−2.53)	3.35 (−3.71)	3.37 (−3.83)				3.05–3.22[18]
$S = 0$	2.30 (0.00)	2.44 (0.00)	2.43 (0.00)				
$S = 2$	2.78 (−1.46)	2.91 (−2.20)	2.92 (−2.26)				
$S = 3$	3.25 (−2.53)	3.37 (−3.71)	3.38 (−3.83)				
$Mo_2Cl_9^{3-}$							
broken symmetry	2.29 (0.00)	3.34 (−0.52)	3.45 (−0.64)				2.53–2.78[23]
$S = 0$	2.29 (0.00)	2.40 (0.00)	2.36 (0.00)				
$S = 2$	2.87 (+0.41)	2.96 (−0.22)	2.96 (−0.29)				
$S = 3$	3.46 (+0.69)	3.57 (−0.46)	3.58 (−0.59)				
$W_2Cl_9^{3-}$							
broken symmetry	2.40 (0.00)	3.05 (−0.17)	3.08 (−0.25)	2.36 (0.00)	2.39 (0.00)	2.39 (0.00)	2.42–2.50[19]
$S = 0$	2.40 (0.00)	2.46 (0.00)	2.46 (0.00)	2.36 (0.00)	2.39 (0.00)	2.39 (0.00)	
$S = 2$	2.91 (+0.61)	3.00 (+0.01)	3.00 (−0.05)	2.88 (+1.08)	2.93 (+0.31)	2.94 (+0.42)	
$S = 3$	3.52 (+1.10)	3.63 (0.00)	3.64 (−0.14)	3.50 (+1.80)	3.59 (+0.54)	3.60 (+0.57)	
$Re_2Cl_9^{1-}$							
broken symmetry	2.79 (−0.04)	3.34 (−0.54)	3.42 (−0.63)	2.41 (0.00)	2.87 (−0.15)	2.97 (−0.20)	2.71[21,22]
$S = 0$	2.49 (0.00)	2.56 (0.00)	2.56 (0.00)	2.40 (0.00)	2.45 (0.00)	2.46 (0.00)	
$S = 2$	2.85 (+0.03)	2.94 (−0.40)	2.94 (−0.44)	2.81 (+0.40)	2.87 (−0.04)	2.88 (−0.08)	
$S = 3$	3.36 (+0.31)	3.48 (−0.50)	3.49 (−0.59)	3.35 (+0.89)	3.46 (+0.04)	3.47 (−0.07)	

[a] Energies of the states (eV), relative to $S = 0$, are shown in parentheses.

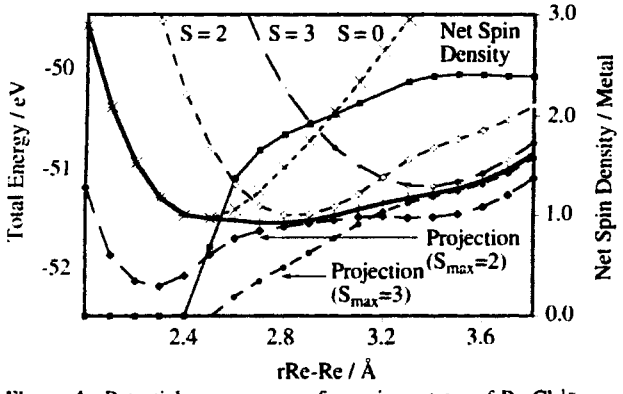

Figure 4. Potential energy curves for various states of $Re_2Cl_9^{1-}$.

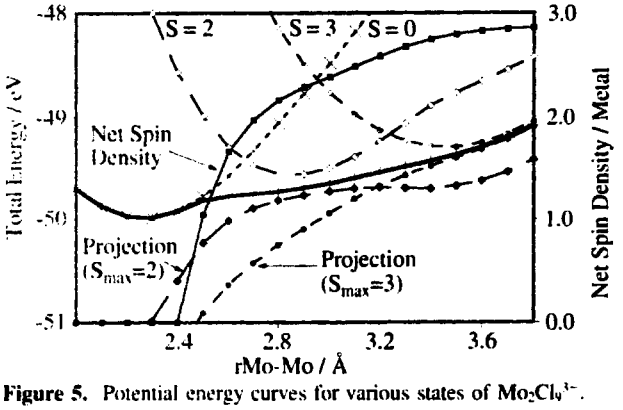

Figure 5. Potential energy curves for various states of $Mo_2Cl_9^{3-}$.

confirming that spin projection does not give rise to any new features in the potential energy curve.

$Re_2Cl_9^{1-}$. The Re–Re separation in the $Re_2Cl_9^{1-}$ anion was reported as long ago as 1971,[21] but a full crystal structure has only recently appeared in the open literature.[22] The metal–metal separation is 2.714 Å, over 0.2 Å longer than that in the neighboring tungsten complex. The features of the LDA curve (Figure 4) for $Re_2Cl_9^{1-}$ are qualitatively very similar to those shown for $W_2Cl_9^{3-}$ in Figure 3. We can again identify three distinct regions of the curve corresponding to weak antiferromagnetic coupling of all metal-based electrons (rRe–Re > 3.2 Å), delocalization of the σ electrons in isolation (2.7 Å < rRe–Re < 3.2 Å), and finally full delocalization where rRe–Re < 2.6 Å. In the appropriate intervals, the associated $S = 0$, 2, and 3 curves again lie close and parallel to the broken-symmetry curve. In contrast to the two previous examples, the relative ordering in $Re_2Cl_9^{1-}$ is $S = 0 \approx S = 2 < S = 3$, and the global minimum on the broken-symmetry curve corresponds to the antiferromagnetically coupled counterpart of the $S = 2$ state, where a single Re–Re σ bond is present. The equilibrium Re–Re separation is 2.79 Å, in excellent agreement with the experimentally determined value of 2.71 Å. Similar conclusions regarding the ground-state electronic structure were reached in a recent paper using the SCF-Xα-SW method.[22] We note, however, that the potential energy curve is very flat in the region of the minimum, due to the energetic proximity of the $S = 0$ and $S = 2$ states, and so delocalization of the δ_π electrons is a energetically facile process. We therefore anticipate that the geometry and magnetic properties of the $Re_2Cl_9^{1-}$ anion may be very sensitive to environmental perturbations. We will return to this point in the discussion of $Mo_2Cl_9^{3-}$. The rhenium and tungsten species are isoelectronic complexes, and it is instructive to consider the reasons for the significant differences between the two. The higher charge on the Re^{4+} ion leads to a contraction of the metal-based orbitals, and hence reduces the overlap of metal-based orbitals relative to $W_2Cl_9^{3-}$. The 5d orbitals of Re^{4+} clearly remain sufficiently diffuse to allow delocalization of the σ electrons but not their δ_π counterparts.[20,22]

The features of the spin-projected curves are very similar to those previously described for $Cr_2Cl_9^{3-}$ and $W_2Cl_9^{3-}$. Projections using $S_{max} = 2$ and $S_{max} = 3$ again have limited regions of validity (where the corresponding ferromagnetic states lie close to the broken-symmetry ground state), and in these regions the spin-projected curve closely follows the broken-symmetry ground state. It is interesting to note that the spin-projected curve using $S_{max} = 2$ exhibits two minima, at approximately 2.3 and 3.4 Å, and the double-well shaped curve is very similar to that previously reported for Cr_2.[5a] Similar double minima are also present in the spin-projected ($S_{max} = 2$) curves for $W_2Cl_9^{3-}$ (at 2.1 Å and 3.5 Å) and for $Cr_2Cl_9^{3-}$ (below 1.8 Å and at 3.4 Å), but in these cases, the minima lie outside the energy range shown in Figures 2 and 3. The prior discussion of the validity of eq 3, along with the available structural data, clearly indicates that these secondary minima are simply artifacts of incorrect spin projection.

$Mo_2Cl_9^{3-}$. The $Mo_2Cl_9^{3-}$ anion represents the most structurally versatile of the four species described in this paper, crystallographic data indicating that the Mo−Mo separation can vary over a range of 0.35 Å,[19c, 23] from 2.53 Å in $K_3Mo_2Cl_9$ to 2.78 Å in the corresponding tetramethylammonium salt. This observation suggests that the metal−metal separation is determined by a subtle balance of several factors and is therefore easily perturbed by changes in the crystal environment. The gross features of the LDA potential energy curve shown in Figure 5 are qualitatively similar to those shown for $W_2Cl_9^{3-}$ (Figure 3), with the energy of the associated states increasing in the order $S = 0 < S = 2 < S = 3$. This in turn suggests that the ground state should be fully delocalized with rMo−Mo in the region of 2.35 Å,[24] contrary to the available experimental data. On closer examination, we note that although the ordering of spin states is the same as in $W_2Cl_9^{3-}$, the $S = 0$ and $S = 2$ states lie much closer in energy in the molybdenum complex. Accordingly, the region of the broken-symmetry curve corresponding to the presence of a Mo−Mo σ bond in isolation lies close to the fully-delocalized, triply bonded ground state, giving rise to a plateau in the region 2.6 Å < rMo−Mo < 2.8 Å. This plateau corresponds precisely to the region where most of the experimental structures are clustered, and the weak coupling of the δ_π electrons is consistent with the paramagnetism observed in all salts of $Mo_2Cl_9^{3-}$.[23b]

The most simple explanation for this observation is that in a system such as $Mo_2Cl_9^{3-}$; where the different spin states are closely spaced, the LDA is unable to correctly model their relative stabilities. A second possibility is that the spin-projected pure singlet ground state exhibits an additional minimum which is not present in the broken-symmetry state. Unfortunately the area of most interest, 2.5 < rMo−Mo < 2.8 Å, corresponds to the transition between two distinct regions, and therefore accurate spin projection in this region is not possible. The spin-projections in the other areas do, however, behave exactly as in previous examples, closely following the shape of the broken-symmetry curve. Therefore, while we cannot eliminate the presence of a second minimum in the pure singlet ground-state curve, we feel confident that none exists.

A third possible explanation for the apparent failure of the LDA arises from a consideration of the structural properties of the salts of $Mo_2Cl_9^{3-}$. A linear relationship between cation size and Mo−Mo separation has been established by Stranger and co-workers[19c] and interpreted in terms of steric repulsions between the cations and the bridging halides, which in turn causes an elongation along the trigonal axis. If the effect of the cation is to elongate the Mo−Mo bond, then the shortest known Mo−Mo separation (2.529 Å in $K_3Mo_2Cl_9$) must represent an *upper limit* to the Mo−Mo separation in the gas-phase molecule at 0 K, the conditions to which the current calculations relate. Thus it may be that the Mo−Mo separation in the gas phase is indeed close to 2.35 Å, as Figure 5 indicates, but in the solid state at ambient temperatures the molecule is forced out of the global minimum and into the plateau region of the potential energy curve. This is only possible in $Mo_2Cl_9^{3-}$ because of the energetic proximity of the $S = 0$ and 2 states, a situation which also prevails in $Re_2Cl_9^{1-}$, and hence we anticipate similar structural diversity in salts of this anion. In contrast, cation-dependent structural changes are much less prevalent in salts of $W_2Cl_9^{3-}$, where the separation of the $S = 0$ and 2 associated states is much larger. Gas phase structural data on the triply charged $Mo_2Cl_9^{3-}$ are likely to remain elusive, but solution EXAFS data may provide some insight into this intriguing problem.

Gradient Corrections

The influence of gradient corrections (both BP and PW91) on the potential energy curves of $Cr_2Cl_9^{3-}$, $W_2Cl_9^{3-}$, $Re_2Cl_9^{1-}$, and $Mo_2Cl_9^{3-}$ is summarized in Table 1. Full curves are not shown, but can be constructed assuming that the broken-symmetry curve follows the lowest energy path between the $S = 0$, 2, and 3 associated states. In all cases, the gradient corrections leave the positions of the minima of the associated states essentially unaffected but significantly change their relative energies. Taking the $W_2Cl_9^{3-}$ ion as a representative example, the LDA places $S = 0$ state clearly below both $S = 2$ and $S = 3$, leading to a fully delocalized ground state. In contrast, all three pure spin states have very similar energies with both BP and PW91 functionals, and the global energy minimum for the broken-symmetry state lies in the region of rW−W = 3.05 Å, corresponding to delocalization of the σ electrons but only weak coupling of the δ_π subset. Thus the LDA and gradient-corrected functionals lead to contrasting conclusions regarding the ground state of $W_2Cl_9^{3-}$. The former predicts a triply bonded state with rW−W = 2.40 Å, whereas the latter suggest a system with only a single W−W bond, and rW−W = 3.05 Å. The available structural data clearly indicate that the LDA provides a much better description of the metal−metal bonding than the PW91 functional. Approximate spin projection using the $S_{max} = 2$ and $S_{max} = 3$ where appropriate produces identical conclusions as described previously: the pure singlet ground state closely follows the broken-symmetry curve in all well-defined regions, and no additional minima emerge.

Table 1 indicates that in general the gradient corrections tend to overstabilize states with high spin density. This spin density can either be global, in the sense that the total spin is nonzero ($S = 2$ and 3), or local, as in the regions of the broken-symmetry curve which exhibit full or partial electron localization, where the net spin is zero but the component metal ions have non-zero spin density. For both $Re_2Cl_9^{1-}$ and $Mo_2Cl_9^{3-}$, the gradient-corrected energies of the associated states increases in the order $S = 3 \approx S = 2 < S = 0$, resulting in global minima in the broken-symmetry curve in the vicinity of rM−M = 3.40 Å, corresponding to weak antiferromagnetic coupling of all six metal-based electrons. In both cases, the potential energy curves are very flat in the interval 3.0 < rM−M < 3.5 Å, due to the close proximity of the $S = 3$ and $S = 2$ states, but in any case this range clearly does not compare favorably with the experimentally determined metal−metal separations (2.71 Å for Re, 2.53−2.78 Å for Mo). The equilibrium Cr−Cr separation is less strongly influenced by gradient corrections than the other systems because the fully localized state is the ground state even with the LDA functional. Thus the additional stabilization of this region by gradient corrections does not result in a distinct change in ground-state electronic structure, as it does in the other three complexes. In summary, gradient corrections underestimate the stability of delocalized states, where the metal−metal interactions are relatively strong, and thus tend to overestimate rM−M. In the four systems described in this work, the LDA gives a significantly better estimate of rM−M than either the BP or PW91 functional in every case.

Quasi-Relativistic Effects. Quasi-relativistic (QR) corrections have been shown to provide improved estimates of metal-ligand bond lengths in systems containing heavy-metals,[25] but their influence on metal−metal bonds has not as yet been studied in detail. QR and nonrelativistic (NR) W−W and Re−Re separations are compared in Table 1 for all three functionals. Trial calculations on molybdenum and chromium systems indicate that, as expected, the influence of QR effects was negligible in both cases. As was the case for gradient

corrections, the major influence of the QR effects occurs in the relative energies of the pure spin states, rather than in the positions of their minima. Considering firstly the LDA functional, the inclusion of QR effects results in only a small contraction of the W−W bond, but in contrast *r*Re−Re is reduced from 2.79 to 2.40 Å. The relative energies of the various states indicate that QR corrections cause a 0.37 eV stabilization of the $S = 0$ associated state relative to $S = 2$. As a result, the δ_π electrons delocalize, causing a distinct shift in ground-state electronic structure and, therefore, in metal−metal separation. A similar relative stabilization (0.47 eV) of the $S = 0$ state occurs in the tungsten system, but as the δ_π electrons are already delocalized even in the absence of QR effects, no significant shift in *r*W−W occurs. The crystal structure of $Re_2Cl_9^{1-}$ suggests that, in conjunction with the LDA, QR corrections overestimate metal−metal bonding, thus providing a poorer estimate of the metal−metal separation in $Re_2Cl_9^{1-}$. The QR LDA potential energy curve is, however, very flat for this system, and it is unclear whether the poor result is caused by approximations in the functional, the QR correction, or a combination of both.

It is noteworthy that the gradient and QR corrections have opposite effects: the former underestimate the significance of metal−metal bonding while the latter overestimate it. The question naturally arises whether a combination of both could provide an accurate description of the systems described in this work. Accordingly, the results of gradient-corrected QR calculations on both $W_2Cl_9^{3-}$ and $Re_2Cl_9^{1-}$ are also summarized in Table 1. The two effects are indeed compensatory, and the net result is that, in $W_2Cl_9^{3-}$, the fully delocalized ground state is recovered when both QR corrections and gradient corrections are included. In $Re_2Cl_9^{1-}$, the QR PW91 estimate of *r*Re−Re, 2.87 Å, is significantly better than the NR value, and only marginally worse than the original LDA value. In the absence of detailed experimental data on the potential energy curves, however, it is difficult to further evaluate the relative merits of the QR PW91 (or BP) and NR LDA results.

Before leaving the subject of relativistic effects, we would like to emphasize that the quasi-relativistic correction applied here does not take into account spin−orbit coupling. In a system such as $W_2Cl_9^{3-}$, where the $S = 0$ state clearly lies much lower than either of the other associated states, the additional effects of spin-orbit coupling are unlikely to change the nature of the ground state. This is not, however, the case for $Re_2Cl_9^{1-}$, where the energies of the associated states are very similar. In this case, the application of a full relativistic correction, with or without gradient corrections, may reveal new features in the potential energy curve. We intend to explore this possibility in the future.

Conclusions

For each of the bimetallic systems described in this paper, the potential energy curve for the broken-symmetry state may be divided into three distinct regions based on the nature of the metal−metal bonding. At large metal−metal separations, all the metal-based electrons are localized, and a singlet ground state arises through weak antiferromagnetic coupling between the two centers. As the metal−metal separation is reduced, an intermediate state arises where the σ electrons are delocalized but their δ_π counterparts remain localized. Finally, at short metal−metal distances, all six metal-based electrons delocalize over both centers. In the weakly antiferromagnetically coupled limit the $S = 3$ associated state, corresponding to ferromagnetic coupling of all six metal-based electrons, lies close and parallel to the broken-symmetry curve. Likewise, where the σ electrons are involved in a strong bond but the four δ_π electrons remain weakly coupled, the $S = 2$ associated state will approach the broken-symmetry curve. Finally, in the limit of complete delocalization, the broken-symmetry solution is convergent with the $S = 0$ singlet ground state arising from a calculation performed in full (D_{3h}) symmetry. Thus by considering the relative energies of the three associated states, $S = 0$, 2, and 3, it is possible to clearly identify the distinct regions of the broken-symmetry curve.

The range of internuclear separations over which a particular coupling mode prevails is relatively insensitive to the identity of the metal ion and also to the density functional employed, and it is the relative energies of the different states which determines the ground-state metal−metal separation. The local density approximation results in remarkably good estimates of the equilibrium metal−metal separations in $Cr_2Cl_9^{3-}$, $W_2Cl_9^{3-}$, and $Re_2Cl_9^{1-}$. In contrast, the LDA estimate of *r*Mo−Mo, 2.35 Å, is rather poor compared to experimentally determined values ranging from 2.53 to 2.78 Å. This may simply represent the limitations of approximate density functional theory, but the shape of the potential energy curves suggests an alternative explanation. The $S = 0$ and $S = 2$ associated states lie very close in energy for $Mo_2Cl_9^{3-}$, and consequently there is a plateau region between 2.5 and 2.8 Å, only 0.3 eV higher in energy than the global minimum at *r*M−Mo = 2.35 Å. Thus it may be that in the gas phase, the Mo−Mo separation is indeed short, but in the solid-state the anion is forced out of the global minimum and into the plateau region by the steric requirements of the counterions.

The gradient-corrected BP and PW91 functionals overestimate the metal−metal separation in all three cases, by as much as 0.5 Å in the case of $W_2Cl_9^{3-}$. This error is traced to the overstabilization of high-spin single-ion states, causing the σ and δ_π electrons to localize, even in the tungsten system where experimental data indicates the presence of a strong triple bond. Quasi-relativistic (QR) corrections have the opposite effect to gradient corrections, favoring the delocalization of metal-based electrons and hence short metal−metal bond lengths. At the LDA level, QR effects have little effect on the W−W separation in $W_2Cl_9^{3-}$, where all valence electrons are already delocalized, but cause the δ_π electrons in $Re_2Cl_9^{1-}$ to delocalize, resulting in a 0.39 Å contraction in the Re−Re bond and significantly poorer agreement with experiment. The effects of gradient and QR effects are to some extent compensatory, but in no case does a combination of the two give a better estimate of *r*M−M than the simple nonrelativistic LDA functional.

Approximate spin-projection techniques were used to extract pure singlet ground-state energies from the broken-symmetry states. In order to perform this approximate spin-projection, it is necessary to determine which electrons are weakly coupled, and hence the maximum spin attainable, S_{max}. The identification of the $S = 2$ and $S = 3$ states as the ferromagnetic counterparts of the broken-symmetry state in different regions of the curve allows the choice of S_{max} to be made in a rational manner. It is valid to consider all six metal-based electrons as weakly coupled and therefore to employ $S_{max} = 3$ in the projection procedure, *only* where the $S = 3$ curve lies close and approximately parallel to the broken-symmetry curve. Likewise, spin-projection using $S_{max} = 2$ is valid *only* when the $S = 2$ and broken-symmetry curves lie parallel and close together. Finally, when the $S = 0$ associated state converges with the broken-symmetry curve, no correction is required. Since a requirement for valid spin projection is that the broken-symmetry and high-spin curves must lie close and parallel to each other, it therefore follows that the spin-projected singlet ground state must closely follow

the broken-symmetry curve at all rM−M, and no new minima can arise in the spin-projected ground state. If, however, the spin projection is performed using an inappropriate value of S_{max} (*i.e.*, where the corresponding high-spin state lies far from the broken-symmetry curve), then the energy of the ground state will necessarily be overestimated, and additional minima will emerge in the spin-projected curve as artifacts of the incorrect choice of S_{max}. If unusual features do appear in the potential energy curve for a spin-projected ground state, it is therefore crucial to critically evaluate whether the chosen value of S_{max} is appropriate in the region of interest. Finally, we reemphasize that the detailed discussion of spin-projected ground states presented here is not intended to establish the procedure as one of general utility. Given the imprecise way of linking the different segments of the spin-projected curve together, the generation of a continuous ground-state curve remains far from simple. In fact, the most important conclusion is that, when considering the general features of a potential energy curve, approximate spin projection is not necessary, because the broken-symmetry curve lies close to that for the true ground state at all points.

Acknowledgment. We express our gratitude to the Australian Research Council (ARC) for financial support and the EPSRC (UK) for a scholarship to T.L.

References and Notes

(1) (a) Cotton, F. A.; Walton, R. A. *Multiple Bonds Between Metal Atoms*; Oxford University Press: Oxford, U.K., **1993** (references therein).

(2) (a) Ginsberg, A. *J. Am. Chem. Soc.* **1980**, *102*, 111. (b) Bursten, B. E.; Cotton, F. A.; Fang, A. *Inorg. Chem.* **1983**, *22* , 2127. (c) Heath, G. A.; McGrady, J. E. *J. Chem. Soc., Dalton. Trans.* **1994**, 3767. (d) Gheller, S. F.; Heath, G. A.; Hockless, D. C. R.; Humphrey, D. G.; McGrady, J. E. *Inorg. Chem.* **1994**, *33*, 3986. (e) Kennedy, B. J.; Heath, G. A.; Khoo, T. J. *Inorg. Chim. Acta* **1991**, *190*, 265. (f) Cotton, F. A.; Feng, X. *Int. J. Quantum Chem.* **1996**, *58*, 671.

(3) Noodleman, L.; Norman, J. G., Jr. *J. Chem. Phys.* **1979**, *70*, 4903.

(4) Andzelm, J.; Wimmer, E. *J. Chem. Phys.* **1992**, *96*, 1280.

(5) (a) Edgecombe, K. E.; Becke, A. D. *Chem. Phys. Lett.* **1995**, *244*, 427. (b) Delley, B.; Freeman, A. J.; Ellis, D. E. *Phys. Rev. Lett.* **1985**, *54*, 661. (c) Baykara, N. A.; McMaster, B. N.; Salahub, D. R. *Mol. Phys.* **1984**, *52*, 891. (d) Dunlap, B. I. *Phys. Rev. A.* **1983**, *27*, 2217.

(6) (a) Medley, G. A.; Stranger, R. *Inorg. Chem.* **1994**, *33*, 3976. (b) Brown, C. A.; Remar, G. J.; Musselman, R. L.; Solomon, E. I. *Inorg. Chem.* **1995**, *34*, 688. (c) Mouesca, J. -M.; Chen, J. L.; Noodleman, L.; Bashford, D.; Case, D. A. *J. Am. Chem. Soc.* **1994**, *116*, 11898. (d) Noodleman, L.; Case, D. A. *Adv. Inorg. Chem.* **1992**, *38*, 423. (e) Jacobsen, H.; Kraatz, H. B.; Ziegler, T.; Boorman, P. M. *J. Am. Chem. Soc.* **1992**, *114*, 7851. (f) Ross, P. K.; Solomon, E. I. *J. Am. Chem. Soc.* **1991**, *113*, 3246. (g) Bencini, A. Gatteschi, D. *J. Am. Chem. Soc.* **1986**, *108*, 5763. (h) Noodleman, L.; Baerends, E. J. *J. Am. Chem. Soc.* **1984**, *106*, 2316. (i) Aizman, A.; Case, D. A. *J. Am. Chem. Soc.* **1982**, *104*, 3269.

(7) Lovell, T.; McGrady, J. E.; Stranger, R.; Macgregor, S. A. *Inorg. Chem.* **1996**, *35*, 3079.

(8) Trogler, W. C. *Inorg. Chem.* **1980**, *19*, 697.

(9) Ziegler, T. *Chem Rev.* **1991**, *91*, 651.

(10) (a) Baerends, E. J.; Ellis D. E.; Ros, P. *Chem. Phys.* **1973**, *2*, 42. (b) Baerends, E. J.; Ros, P. *Int. J. Quantum Chem.* **1978**, *S12*, 169. (c) teVelde, G.; Baerends, E. J. *J. Comput. Phys.* **1992**, *99*, 84.

(11) Vosko, S. H.; Wilk, L.; Nusair, M. *Can. J. Phys.* **1980**, *58*, 1200.

(12) Becke, A. D. *Phys. Rev. A* **1988**, *38*, 3098.

(13) Perdew, J. P. *Phys. Rev. B* **1986**, *33*, 8822; *34*, 7406.

(14) Perdew, J. P.; Chekavry, J. A.; Vosko, S. H.; Jackson, K. A.; Pederson, M. R.; Singh, D. J.; Fioihais, C. *Phys. Rev. B* **1992**, *46*, 6671.

(15) (a) Ziegler, T.; Snijders, J. G.; Baerends, E. J. *J. Chem. Phys.* **1981**, *74*, 1271. (b) Ziegler, T.; Baerends, E. J.; Snijders, J. G.; Ravenek, W. *J. Phys. Chem.* **1989**, *93*, 3050.

(16) Versluis, L.; Ziegler, T. J. *Chem. Phys.* **1988**, *88*, 322.

(17) Noodleman, L. *J. Chem. Phys.* **1981**, *74*, 5737.

(18) (a) Saillant, R.; Wentworth, R. A. D. *Inorg. Chem.* **1968**, *7*, 1606. (b) Wessel, G. J.; Ijdo, D. J. W. *Acta Crystallogr.* **1957**, *10*, 466. (c) Grey, I. E.; Smith, P. W. *Aust. J. Chem.* **1971**, *24*, 73.

(19) (a) Dunbar, K. R.; Pence, L. E. *Acta Crystallogr.* **1991**, *C47*, 23. (b) Watson, W. H., Jr.; Waser, J. *Acta Crystallogr.* **1958**, *11*, 689. (c) Stranger, R.; Grey, I. E.; Madsen, I. C.; Smith, P. W. *J. Solid State Chem.* **1987**, *69*, 162.

(20) McGrady, J. E.; Stranger, R.; Lovell, T. *Inorg. Chem.* **1997**, *36*, 3242.

(21) Stokeley, P. F. Ph.D. Thesis, Massachussetts Institute of Technology, Cambridge, 1969.

(22) Heath, G. A.; McGrady, J. E.; Raptis, R. G.; Willis, A. C. *Inorg. Chem.*, **1996**, *35*, 6838.

(23) (a) Saillant, R.; Jackson, R. B.; Streib, W.; Folting, K.; Wentworth, R. A. D. *Inorg. Chem.* **1971**, *10*, 1453. (b) Stranger, R.; Smith, P. W.; Grey, I. E. *Inorg. Chem.* **1989**, *28*, 1271.

(24) In a previous paper we reported a minimum at rM−Mo = 2.71 Å.[7] A detailed analysis of the potential energy curve indicates that, while the curve is very flat in this region, no minimum is present.

(25) Schreckenbach, G.; Ziegler, T.; Li, J. *Int. J. Quantum Chem.* **1995**, *56*, 477.